The Influence of Land Surface Properties on Sahel Climate. Part I: Desertification

YONGKANG XUE AND JAGADISH SHUKLA

Center for Ocean–Land–Atmosphere Studies, Calverton, Maryland

(Manuscript received 18 June 1992, in final form 12 April 1993)

ABSTRACT

This is a general circulation model sensitivity study of the physical mechanisms of the effects of desertification on the Sahel drought. The model vegetation types were changed in the prescribed desertification area, which led to changes in the surface characteristics. The model was integrated for three months (June, July, August) with climatological surface conditions (control) and desertification conditions (anomaly) to examine the summer season response to the changed surface conditions. The control and anomaly experiments consisted of five pairs of integrations with different initial conditions and/or sea surface temperature boundary conditions.

In the desertification experiment, the moisture flux convergence and rainfall were reduced in the test area and increased to the immediate south of this area. The simulated anomaly dipole pattern was similar to the observed African drought patterns in which the axis of the maximum rainfall shifts to the south. The circulation changes in the desertification experiment were consistent with those observed during sub-Saharan dry years. The tropical easterly jet was weaker and the African easterly jet was stronger than normal. Further, in agreement with the observations, the easterly wave disturbances were reduced in intensity but not in number. Descending motion dominated the desertification area. The surface energy budget and hydrological cycle were also changed substantially in the anomaly experiment.

1. Introduction

The sub-Sahara is a semiarid area located between the Sahara desert to the north and the savanna lands to the south (roughly between 10°N and 20°N) and extending from the Atlantic Ocean eastward to Ethiopia. The term "sub-Sahara" will be used interchangeably with "Sahel" in this paper. The sub-Sahara is characterized by the strong seasonality of the climate with a short rainy season in the boreal summer. The Sahel climate is currently dominated by the drought that started during the late 1960s. The drought has lasted for more than 20 years and shows no sign of ending.

According to Nicholson (1979) and Lamb (1978), there have been several drought periods followed by wet episodes in African history. There is some evidence linking the patterns of alternating wet and dry episodes to the sea surface temperature (SST) anomalies in the Atlantic Ocean (Lamb 1978). Lamb found that a distinctive tropical Atlantic SST anomaly pattern (positive anomaly to the south of approximately 10°N; negative anomaly between 10° and 25°N) is associated with the West African drought. Folland et al. (1986) and Semazzi et al. (1988) broadened their investigations to include much of the world's oceans. Folland et al. (1991) found that the relatively modest variations observed in the large-scale patterns of SST have had a substantial impact on the variations of Sahel rainfall. The tropical oceans, on the whole, have considerably more influence than the extratropical oceans. They also found that warmer SST in the Southern Hemisphere, relative to that in the Northern Hemisphere, has been associated with the Sahel drought.

There has also been considerable interest in the relationship between land surface effects and the Sahel drought. In Charney's (1975) pioneering work on the effects of albedo on the African climate, he found that increases of albedo cause a reduction in precipitation. This discovery was confirmed by a number of studies with different models (Chervin 1979; Sud and Fennessy 1982; Laval and Picon 1986). The effects of soil moisture and evaporation have also been investigated in modeling experiments (Walker and Rowntree 1977; Shukla and Mintz 1982; Sud and Fennessy 1984; Yeh et al. 1984; Cunnington and Rowntree 1986; and Rowell and Blondin 1990). Most of these studies showed that less initial soil moisture would lead to less precipitation. Furthermore, the combined effects of surface albedo and soil moisture have also been studied (Sud and Molod 1988; Kitoh et al. 1988). Kitoh et al. (1988) found that the combined effect of surface albedo and soil moisture was nearly equal to the sum of the albedo and soil moisture effects. These modeling studies consistently demonstrate that the land surface has a significant impact on the Sahel climate.

Corresponding author address: Dr. Yongkang Xue, Center for Ocean–Land–Atmosphere Studies, 4041 Powder Mill Rd., Suite 302, Calverton, MD 20705.

However, in most of these sensitivity studies, the area associated with land surface changes and the magnitude of the changes in the surface characteristics, such as albedo and soil moisture, were somewhat arbitrary. All the studies showed a positive feedback between initial soil moisture and rainfall with the exception of one study by Sud and Fennessy (1984). Conflicting opinions have also been expressed on the magnitude of changes in albedo. Analyzing satellite observations, Norton et al. (1979) found that the albedo in West Africa increased during the period 1967 to 1973. During the wet seasons, the albedo changed from 0.23 in 1969 to 0.33 in 1973. Courel et al. (1984), also using satellite observations, found that the albedo was reduced by 0.1 in the Sahel (mainly in the Ferlo and Goudo regions) from 1973 to 1979. The variation range of 0.1 in both studies was far less than the dramatic changes that were made in some of the modeling studies.

Despite the controversy regarding the albedo change, it is commonly recognized that desertification has been occurring in Africa. According to Skoupy (1987) and Lanly (1982), for almost half a century, and particularly over the past 30 years, the vegetation cover has been increasingly degraded across the African continent, with the possible exception of central Africa and some countries bordering the Gulf of Guinea. This has been caused by many factors, such as overexploitation of land resources by overgrazing, poor irrigation, and the destruction of woody vegetation. The annual rate of forest clearing is around 4% for all of West Africa. The savanna, which occupies a vast area in West and central Africa and the large part of the eastern horn, has also been experiencing degradation. In the early 1980s, only 35% of the area of formerly productive savanna was left. In 1983 alone, 4.125 million square kilometers were affected by desertification (Skoupy 1987). Since the physical protection provided by plants is of great importance to the soil, it follows that the destruction of plants has probably damaged the soil layer also.

All the aforementioned modeling studies used simple surface-layer models and changed one parameter at a time to test the model sensitivity. The real desertification process is much more complex and involves a large number of parameters. It is desirable, based upon the previous studies, to explore the land surface effects synergistically. This can only be accomplished with more sophisticated surface models. A two-dimensional (zonal mean) atmospheric model coupled with a biosphere model was used to study the physical mechanisms of the biogeophysical feedback of the land surface on the African climate (Xue et al. 1990; Xue 1991). With this coupled model, two tests involving the removal and expansion of the Sahara desert were performed. The results demonstrated the importance of incorporating the physics of a vegetation layer in the atmospheric model and encouraged further experiments to more realistically study the effects of the land surface on the Sahel drought.

To have a better and more realistic understanding of land surface effects, we have utilized a biophysically realistic surface model (Sellers et al. 1986) with a high-resolution global climate model. The simple biosphere model (SiB) was implemented in the Center for Ocean–Land–Atmosphere Interaction General Circulation Model (COLA GCM) by Sato et al. (1989), and simplified by Xue et al. (1991). In this experiment, we have changed the land surface condition in the Sahel and nearby area into desert and investigated its impact on the model climatology. In section 2, we will briefly describe the model. The designation of desertification scenarios will be presented in section 3. The results from numerical experiments will be presented in section 4. The impact of desertification on rainfall and its significance will be discussed in section 4a. Section 4b will show the effects of desertification on the circulation. In section 4c the surface energy balance and surface hydrology budgets are discussed. The summary and discussion will be given in section 5.

2. Model description

The model used in this study is the COLA GCM, which is a modified version of the National Meteorological Center (NMC) global spectral model. A detailed description of the model dynamics is presented in Sela (1980) and the initialization procedures and boundary conditions are discussed by Kinter et al. (1988). The model has a horizontal rhomboidal truncation at wavenumber 40. The size of each grid box in the transform grid domain is approximately 1.8° (latitude) $\times$ 2.8° (longitude). The vertical coordinate is σ (normalized pressure) which is discretized into 18 levels. Different from an earlier version of the COLA GCM (Sato et al. 1989), the specific humidity is predicted in all 18 layers. The parameterizations for physical processes include the following.

1) An efficient radiation scheme (Harshvardhan et al. 1987). It contains a longwave radiation scheme (Harshvardhan and Corsetti 1984), and a shortwave radiation scheme based on Lacis and Hansen (1974) as modified by Davies (1982). An interactive cloud scheme similar to the one developed by Slingo (1987) is used for the radiation calculation (Hou 1990).

2) The level 2.0 second-order turbulence closure model of Mellor and Yamada (1982), which is used to calculate the vertical diffusion of heat, momentum, and moisture.

3) A modified Kuo scheme for convection and large-scale precipitation (Sela 1980; Kuo 1965; Philips 1979).

4) The simplified SiB (SSiB) (Xue et al. 1991). The model has one vegetation canopy layer and three soil layers, and includes seven prognostic variables: soil wetness in the three soil layers; temperatures of the

canopy, surface, and deep soil; and the water storage on the canopy. The structure of this model is shown in Fig. 1. In this model, the global vegetation distribution is categorized into 12 different biomes (Dorman and Sellers 1989), each with soil and vegetation characteristics specified in some detail. There are 23 parameters in the SSiB that were specified according to the vegetation types. The vegetation map for sub-Sahara is depicted in Fig. 2. In this map, type 1 is tropical rain forest, type 2 is broadleaf deciduous trees, type 6 is broadleaf trees with ground cover, type 8 is broadleaf shrubs with ground cover, type 9 is broadleaf shrubs with bare soil, and type 11 is bare soil.

3. Experimental design for desertification

Since the term "desertification" was introduced by Aubreville (1949), a number of definitions for this concept have evolved. For example, some definitions emphasize the economical impacts, and others refer to it as degradation of land form and destruction of vegetation cover (Verstraete 1986). There are also controversies concerning the degree and extent of desertification in the Sahel. In our desertification experiment, the vegetation types in the area shown in Fig. 2 were replaced by vegetation type 9, which is broadleaf shrubs with bare soil. It generally reflects the degradation of vegetation and soil in this area and the expansion of desert landscapes. The choice of desertification area in our experiment was motivated by Dregne's work (1977). He divided the degree of desertification into four classes: slight, moderate, severe, and very severe. The area we chose corresponds approximately to the area characterized as a severe desertification region in his paper. The area with changed vegetation types shown in Fig. 2 will be referred to as the "test area" in the remainder of this paper.

In the SiB model, different vegetation types are distinguished by the different values of their vegetation parameters, such as vegetation cover and leaf area index; soil properties, such as soil depth, soil wetness at saturation, and hydraulic conductivity of saturated soil; and other morphological, physiological, and physical properties, such as roughness length and albedo. Table 1 shows these properties for the vegetation types in the northern African region. The values of the same parameter for different vegetation types provide a quantitative measure of changes introduced in our experiment.

The vegetation type change in the desertification experiment reduced the vegetation cover, leaf area index, roughness length, soil depth, and degraded other vegetation and soil properties. It was used to represent the destruction of the plants and erosion of the soil after desertification. The albedo was increased by about 0.09 in the test area. The surface albedo has a diurnal variation in the SiB model. Its values shown in Table 1 are 90-day means. These changes are less than those used in previous land surface sensitivity studies, and are also in the range of seasonal and interannual albedo changes, as measured by satellite (Courel et al. 1984, Norton et al. 1979). The soil moisture was also changed in the desertification experiment. As shown in Table 1, vegetation type 9 has sandy soil and thin soil layers. The soil had less capacity to hold water, and the drainage to the deep soil is significant. Since we did not change the initial soil moisture in the areas originally using type 8, where it was already very low, the areas with initial soil moisture changes are smaller than those with albedo changes.

To provide a measure of the response relative to model internal variability, the experiment consisted of several cases with different initial and/or SST boundary conditions. The monthly SST datasets for long-term mean and for four separate years (1950, 1958, 1983, 1984) were obtained from the United Kingdom Meteorological Office (Folland et al. 1991). The year 1958 was a wet year, and 1950 was the wettest year in the Sahel during this century. The years 1983 and 1984 were the driest. The initial and boundary conditions used in our control and anomaly integrations are shown in Table 2. There are five pairs of integrations, and for each pair, the global initial conditions and global SST were identical. The only difference was in the vegetation type and associated land surface properties in the test area shown in Fig. 2. For most of the integrations, June 1988 initial conditions were used because we know from observations (Lamb and Peppler 1991) that seasonal rainfall in 1988 was close to the long-term mean rainfall. The SST values were updated once a day during the course of integrations. Since June, July, and August are the main rainy period in the sub-Sahara area, we integrated the model in each case for three months starting from June. The differences between the ensemble means of the five anomaly integrations and the five control integrations are interpreted as the effects of desertification.

4. Results

a. Rainfall anomaly from desertification experiments

In this section, we will discuss the impact of desertification on rainfall. Figure 3a is the 90-day mean rainfall for the ensemble mean of five control runs. We will refer to the ensembles of the five control and the five desertification integration as C and D, respectively. Figure 3b shows the observed African rainfall climatology from Nicholson (1979). Nicholson's dataset includes all observations collected since early this century. The control runs generally reproduced the main features of climatological rainfall. There is a zonal pattern with three high-rainfall areas in the sub-Sahara region: one in Ethiopia, one on the west coast, and another near the Guinea coast. The strong gradients of rainfall near 15°N and along the equator were well simulated. However, the simulated rainfall in Ethiopia was too

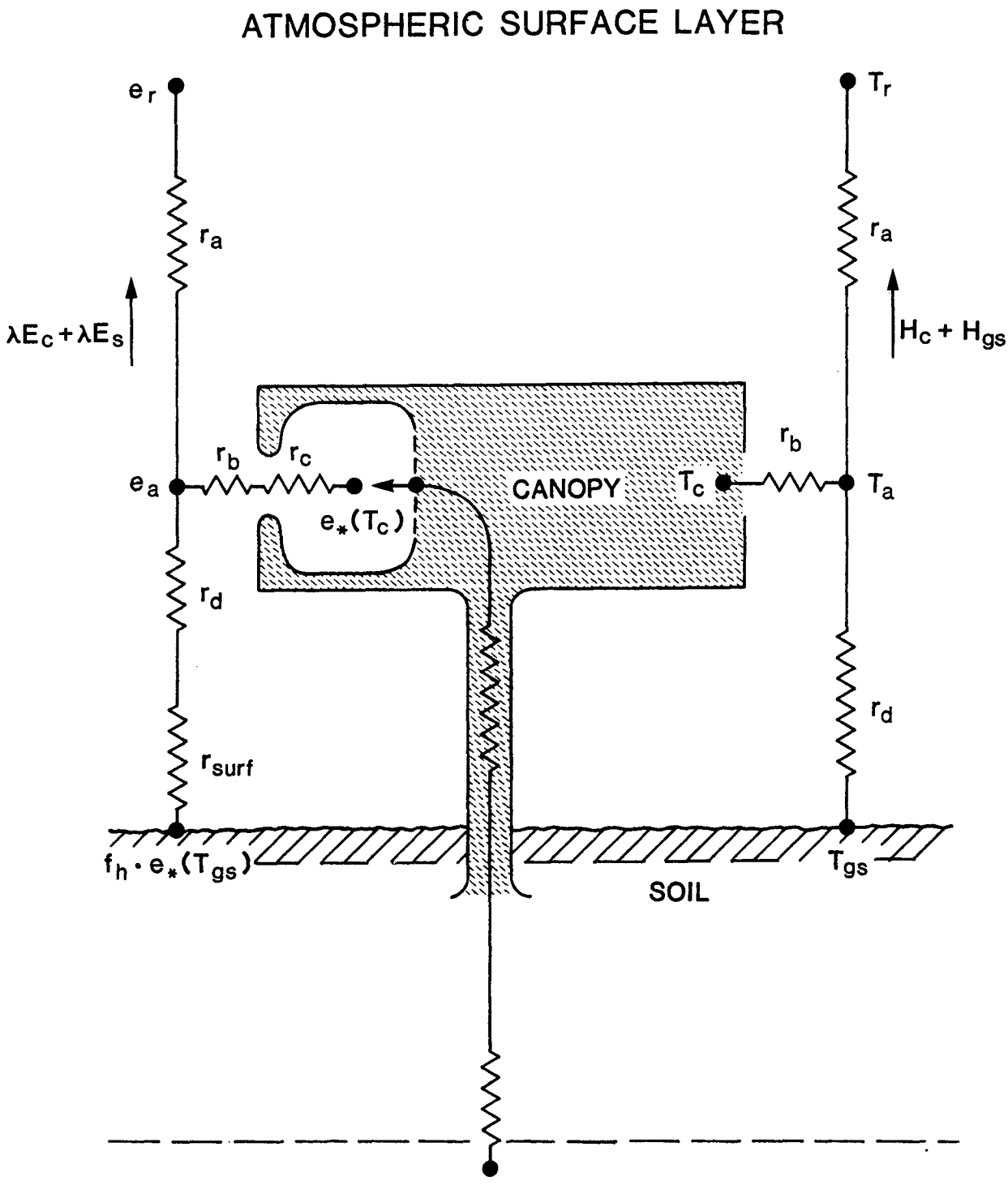

FIG. 1. Schematic diagram of simplified SiB (SSiB). The transfer pathways for latent and sensible heat flux are shown on the left- and right-hand sides of the diagram, respectively. T_r is the air temperature at reference height, T_c the canopy temperature, T_a the air temperature within the canopy space, T_g the soil temperature, r_a the aerodynamic resistance between canopy air space and reference height, r_b the bulk boundary-layer resistance, r_c the bulk stomatal resistance, r_d aerodynamic resistance between canopy air space and ground, and r_{soil} the bare soil surface resistance. H_c and H_{gs} are the sensible heat flux from canopy and ground, respectively. E_c and E_s are the latent heat flux from canopy and ground, respectively.

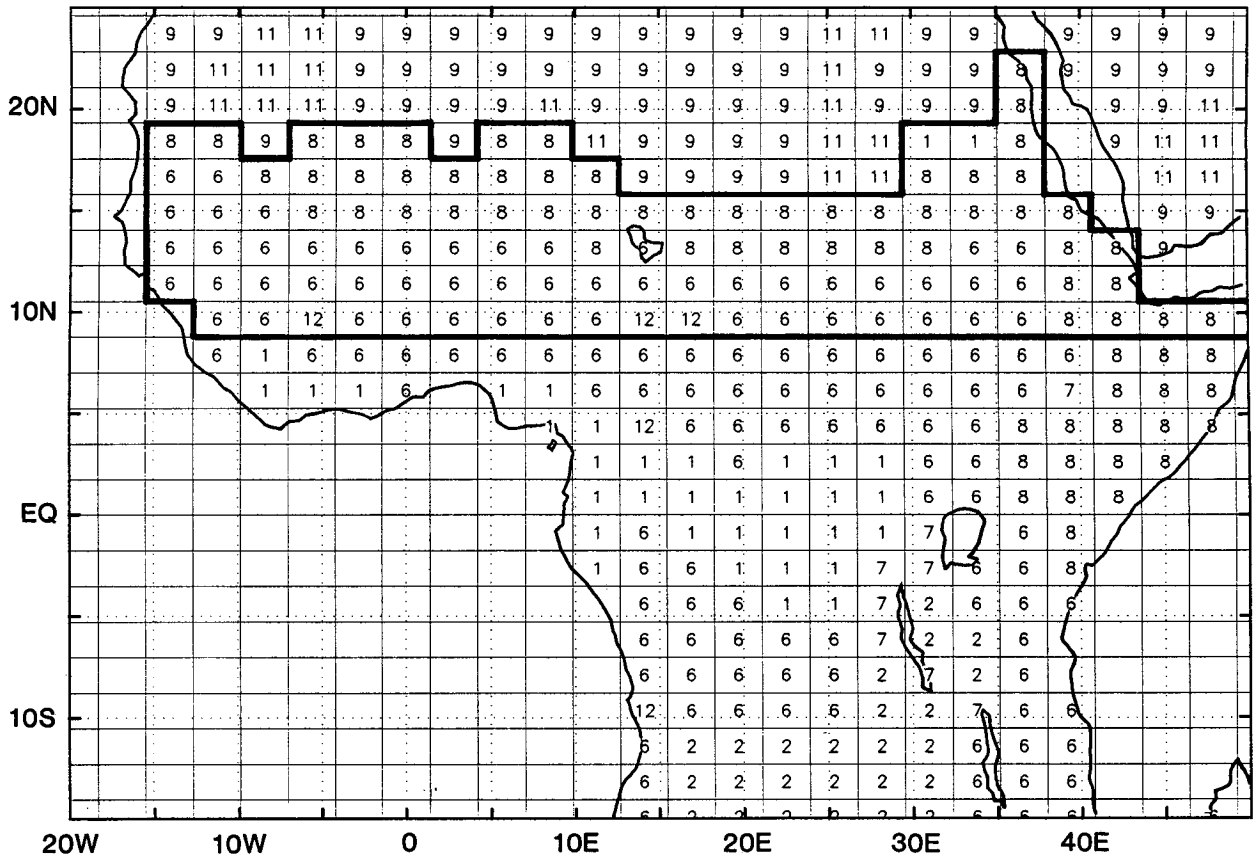

FIG. 2. Vegetation type map for control run. Type 1 is tropical forest. Type 2 is broadleaf-deciduous trees. Type 6 is savanna. Type 7 is grassland. Type 8 is broadleaf shrubs with ground cover. Type 9 is shrub with bare soil. Type 11 is bare soil. Type 12 is crops. In the area enclosed by dark line vegetation types are changed to type 9 for desertification experiment.

high. The rainfall maximum near the Gulf of Guinea was not simulated. Instead, a simulated maximum is located to the north of this region. Generally, the model produced more precipitation than observed. The simulated 1 mm day^{-1} isohyet is located about 2°–4° (one or two model grid boxes) north of its observed position.

TABLE 1. Vegetation parameters for 4 vegetation types.

	Type 6	Type 8	Type 9	Type 11
Mean surface albedo	0.20	0.20	0.30	0.32
Initial soil wetness at test area in control experiment	0.16–0.22	0.05	0.05	0.05
Roughness length (m)				
Jun	0.79	0.20	0.06	
Jul	0.93	0.20	0.06	0.01
Aug	0.97	0.27	0.06	
Depth of three soil layers (m)				
Z_1	0.02	0.02	0.02	0.02
Z_3	1.48	0.47	0.47	0.17
Z_3	2	1	1	0.3
Soil moisture potential at saturation (m)	−0.086	−0.035	−0.035	−0.035
Hydraulic conductivity of saturated soil (m s^{-1})	0.2E-4	0.176E-3	0.176E-3	0.176E-3
Vegetation cover	0.3	0.1	0.1	0
Leaf area index				
Jun	1.42	0.26	0.18	
Jul	2.61	0.26	0.18	0
Aug	5.21	0.81	0.28	

TABLE 2. The initial and boundary conditions.

Case	Initial condition	SST condition	Vegetation types in the test area
C1	1 June 1988	Climatology	As shown in Fig. 2
C2	2 June 1988	Climatology	As shown in Fig. 2
C3	1 June 1987	Climatology	As shown in Fig. 2
C4	1 June 1988	83 SST	As shown in Fig. 2
C5	1 June 1988	50 SST	As shown in Fig. 2
D1	1 June 1988	Climatology	Type 9
D2	2 June 1988	Climatology	Type 9
D3	1 June 1987	Climatology	Type 9
D4	1 June 1988	83 SST	Type 9
D5	1 June 1988	50 SST	Type 9

Figure 4a is the three-month mean rainfall difference in the sub-Sahara region between experiments D and C. Desertification reduced the average rainfall by more than 1.5 mm day^{-1}, about 22% less than the control amount. The West African area had the highest rainfall reduction. There is a clear dipole pattern in this figure.

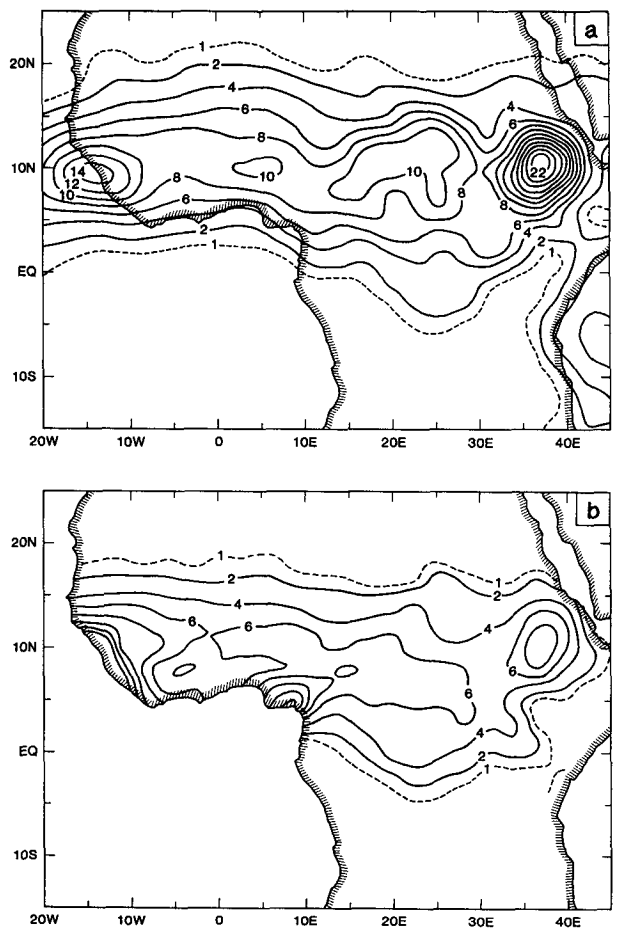

FIG. 3. Three-month mean precipitation. Contour interval is 2 mm day^{-1}. The dash line is 1 mm day^{-1} isohyet: (a) experiment C and (b) observed rainfall climatology (from Nicholson).

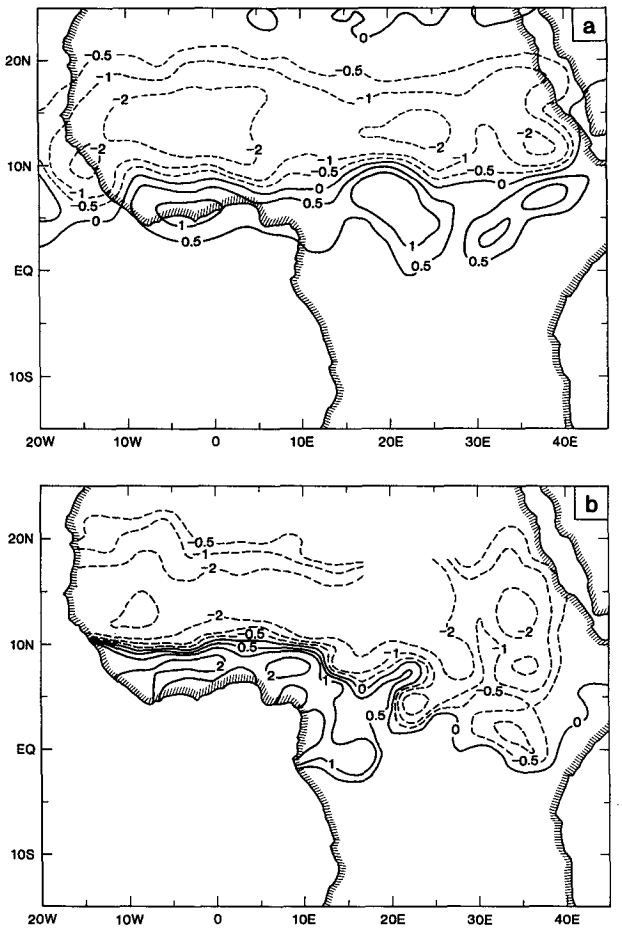

FIG. 4. Three-month mean precipitation. Contour intervals are 0, 0.5, 1, 2, 4 mm day^{-1}: (a) experiment D minus C and (b) observed rainfall differences between the two dry years (1983, 1984) and the two wet years (1950, 1958).

The rainfall was reduced in the test area, but it increased to the immediate south of this region. This pattern was quite similar in all five cases. Based upon the climatological records for Africa, Nicholson (1981) concluded that the rainfall anomalies in the sub-Sahara occur frequently with opposite signs north and south of 10°N. Figure 4b shows the mean observed rainfall differences between the two dry years (1983, 1984) and the two wet years (1950, 1958). The observed anomaly patterns in Fig. 4b are similar to those shown in Fig. 4a. The −0.5 and −1 mm day^{-1} isohyets in both Figs. 4a and 4b have zonal patterns. It can be seen that the zero line in Fig. 4a closely follows the southern boundary of the test area (Fig. 2). This suggests a possible sensitivity to the choice of the desertification area in our experiment. Figure 5 shows a global map of the rainfall difference (D − C), where it can be seen that the main difference is in the sub-Sahara region.

One of the important features of sub-Sahara drought is the displacement of isohyets in some dry years. This

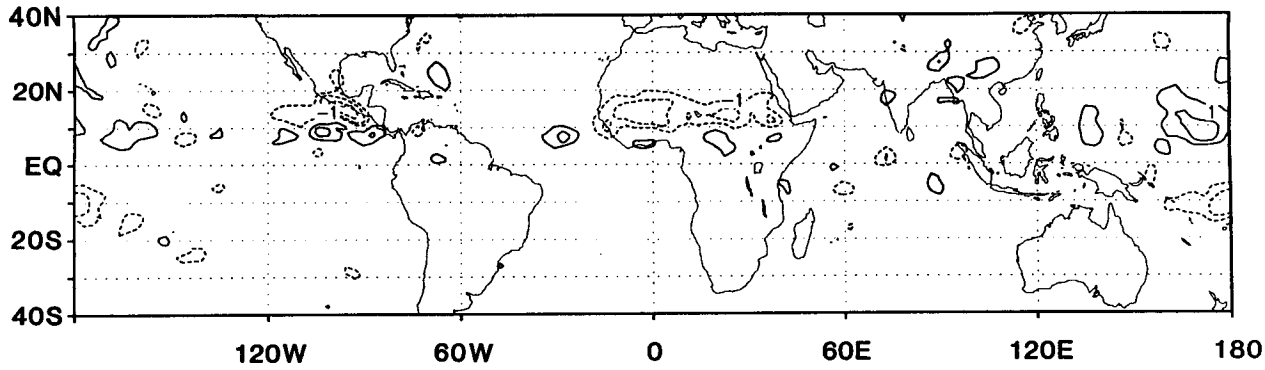

FIG. 5. Three-month mean rainfall of experiment D minus C. Contour intervals are 1, 2, 4 mm day^{-1}.

displacement reduces the rainfall in the Sahel and increases rainfall to the south of 10°N. Figures 6a,b show the zonal average rainfall over the African continent from model simulations (control and desertification) and from observations [average of two wet (1950, 1958) and two dry (1983, 1984) years]. Figure 6b shows that the maximum rainfall was not reduced and that the rainfall deficiency in the Sahel was a consequence of a southward shift of the rainfall maxima. In the model simulation (Fig. 6a), both shifting and reduction of the maximum rainfall contributed to reducing the rainfall over the Sahel.

Figure 7 depicts the time series of 15-day mean rainfall for the average of cases C1, C2, and C3, and the average of cases D1, D2, and D3, over the test area.

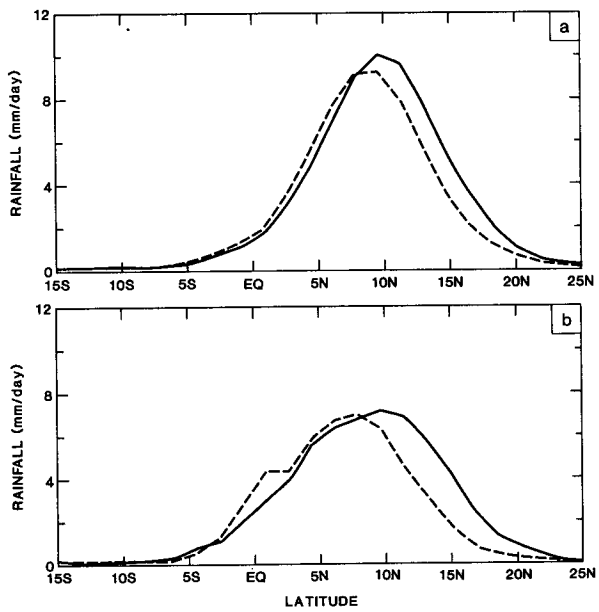

FIG. 6. Zonally averaged rainfall distribution (mm day^{-1}): (a) three-month mean for experiments C (solid line) and D (dash line) and (b) solid line is the mean for 1950 and 1958, dash line is for 1983 and 1984.

The standard deviations for each of the these cases, which varied over the course of the integrations, are also shown in this figure. The average standard deviation is 0.23 mm day^{-1} for desertification cases and 0.11 mm day^{-1} for control cases. In agreement with the observations, the model-simulated rainfall starts to increase in June and reaches its peak in August. In the control case, precipitation increased rapidly during the first 15 days. In the desertification case, however, the rainfall in the first half of the month was nearly constant. Thus, desertification delayed the onset of the rainy season. From the observed data in West Africa during 1940–1983, Dennett et al. (1985) found that throughout the 1970s rainfall was not consistently declining in June of the dry years, although in 1982 and 1983 the early rains did fail. In the desertification case, the rainfall deficiency started to develop in the eastern part of the sub-Sahara during the first 10 days of integration. Subsequently, the reduction of rainfall was more uniformly spread throughout the test area. After 45 days the western part of the test area maintained

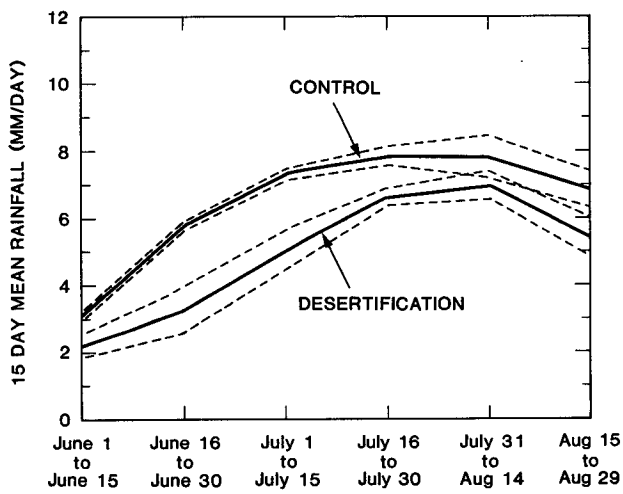

FIG. 7. 15-day mean rainfall (mm day^{-1}) over test area for experiments C and D. Dashed lines define the standard deviation.

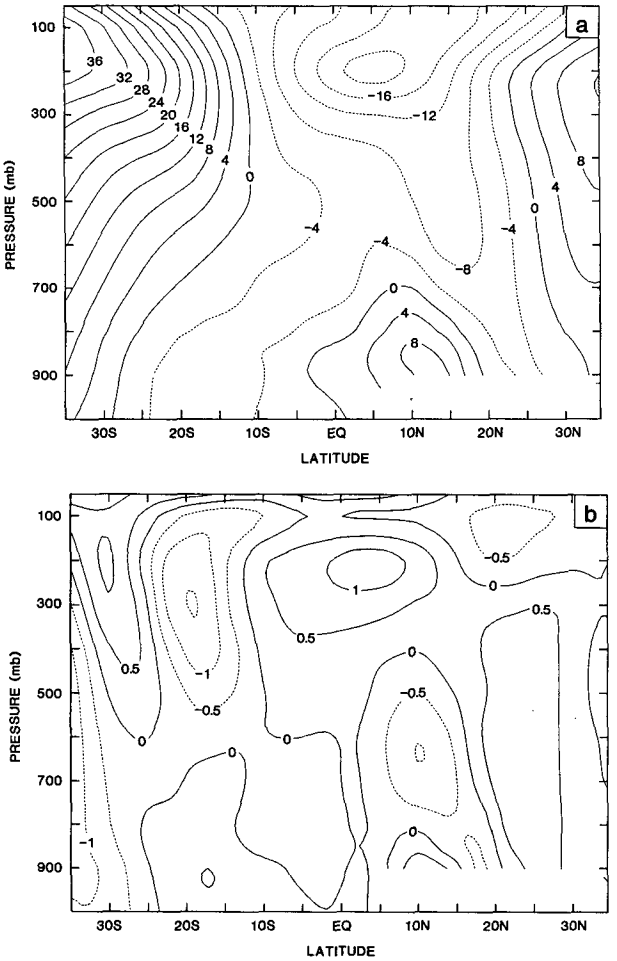

FIG. 8. Zonal averaged zonal velocity (m s^{-1}) over the Africa continent: (a) experiment C and (b) experiments D minus C.

more severe droughts than the east. We also analyzed the rainfall anomaly in the area south of the desertification region, from about 4°N to 8°N. The significant rainfall increase in this region started after about 30 days of integration. This increase was also quite consistent during the following 60 days.

b. Analysis of circulation changes

Large-scale, low-level, moist, southwest airflow and evapotranspiration from the surface are the two main moisture sources for the Sahel rainfall (Druyan and Koster 1989). Any substantial changes of this southwest flow would have a significant impact on rainfall in the Sahel. Kidson (1977) and Newell and Kidson (1984) examined changes in the wind fields associated with Sahelian rainfall variations. Compared with the wind field during wet years (from 1958 to 1962), they found that during the dry years (from 1970 to 1973) the tropical easterly jet (TEJ) at 200 mb was weaker and the African easterly jet (AEJ) at 700 mb near 15°N was stronger. The low-level westerly flow, just north of the equator, was weaker and the Southern Hemisphere middle-latitude westerly jet was stronger in dry years. At and below 700 mb, the meridional wind across the equator into the Northern Hemisphere was weaker during the dry periods.

Figure 8a, which is the zonal wind cross section for experiment C averaged from 15°W to 40°E, shows that the middle-latitude westerlies in both hemispheres, tropical easterlies, and the low-level westerlies north of the equator were well simulated. The 700-mb easterly wind maximum is to the north of the equator. The easterly jet to the south of the equator was not well simulated compared to that shown by Newell and Kidson (1984).

The zonally averaged zonal wind differences (D − C) are presented in Fig. 8b. The low-level westerlies to the north of the equator became weaker in most areas, except near the surface in the test area. The simulated easterlies are weaker at 200 mb and stronger at 700 mb. The changes in the meridional cross section

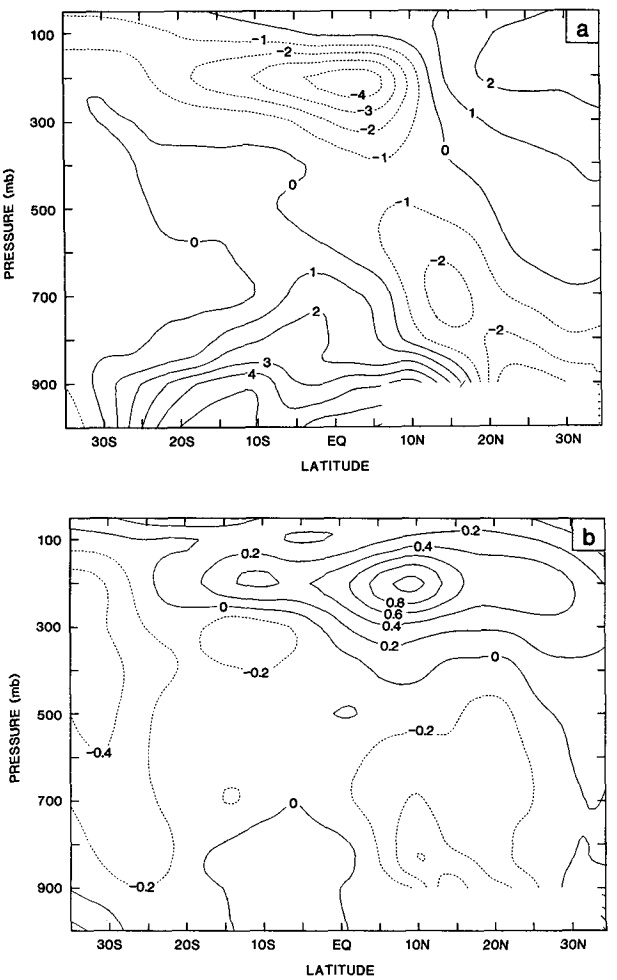

FIG. 9. Zonal averaged meridional winds (m s^{-1}) over the African continent: (a) experiment C and (b) experiments D minus C.

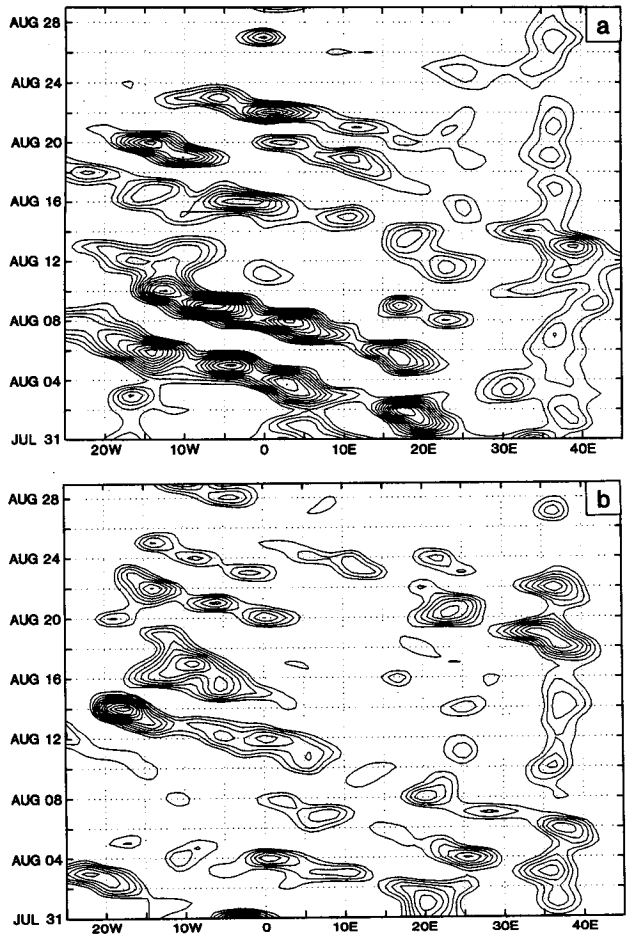

FIG. 10. Time variation of daily rainfall (mm day^{-1}) averaged from 10°N to 18°N. Contour interval is 2 mm day^{-1}. Contours less than 8 mm day^{-1} are eliminated: (a) case C3 and (b) case D3.

along 10°E (not shown) had the same pattern. The zonal wind differences at 850 and 700 mb from our model simulation (not shown) were very similar to those shown by Newell and Kidson (1984) for the zonal wind differences between the African dry and wet years. The magnitudes of the simulated differences, however, were less than those in Newell and Kidson, perhaps due to smaller changes in the simulated surface temperature field, which will be discussed in the following section.

Figures 9a,b are the meridional wind cross sections for experiment C and the differences D − C. Both the northward flow below 700 mb across the equator into the Northern Hemisphere, and the southward flow above 300 mb became weaker in D. The reduction of the northward flow below 700-mb occurred mostly in West Africa. These changes imply a weakening of the monsoon and are in agreement with the circulation anomalies observed in dry years (Kidson 1977; Newell and Kidson 1984).

Figures 10a,b show the time series of August rainfall averaged from 10°N to 18°N for cases C3 and D3, respectively. The isohyets of less than 8 mm day^{-1} are not shown in these figures. In the model simulation, there are more disturbances in August, consistent with the earlier results of Carlson (1969). Figure 10 shows the westward-propagating disturbances, which might originally start from 35°E and intensify as they propagate westward. The wave patterns are well developed west of 20°E. These wave patterns are considered to be the manifestation of the instability of the African easterly jet (Lamb 1983, Reed 1986). Of the six events simulated during August, four reached the west coast of Africa (15°W). With the exception of one event, most disturbances stagnated at the coast and did not continue farther into the Atlantic Ocean. The disturbances have a period of 3–4 days, a phase velocity of about 8° longitude day^{-1}, and a wavelength of about 25° longitude. These features are in reasonable agreement with the observations (Carlson 1969; Burpee 1975). In Fig. 10b, the intensity of disturbances is greatly reduced in the desertification case, although the number of disturbances remained nearly the same. This is more clearly seen from the time series of areally averaged (10°N to 8°N, 8.4°W to 5.6°E) rainfall (Figs. 11a,b) for cases C1 and D1, respectively. This is in good agreement with the earlier study by Reed (1986) who showed that the total number of disturbances over Africa remained the same each year, but fewer strong and/or highly convective disturbances occurred near the coast during periods of extended droughts.

We examined the vertical motion field to investigate the possible causes for the weaker disturbances. The differences in vertical motion (ω) between D and C are shown in Fig. 12. It is clear that above the test area (10°N–18°N) the subsidence became stronger and/or the rising motion became weaker throughout the depth

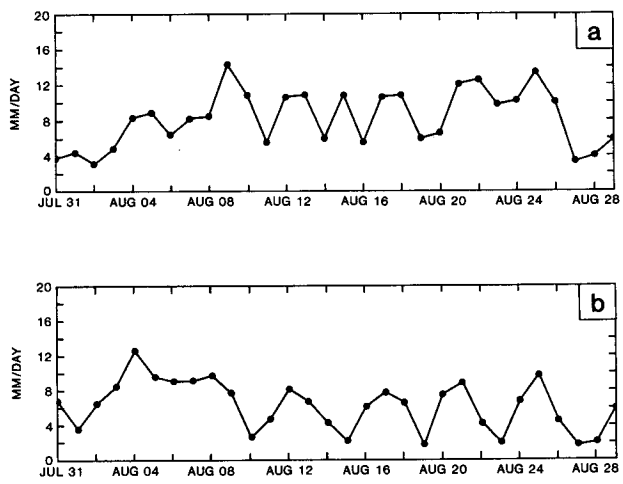

FIG. 11. Daily average rainfall rates (mm day^{-1}) over 10°N to 18°N and 8.4°W to 5.6°E (a) for case C1 and (b) for case D1.

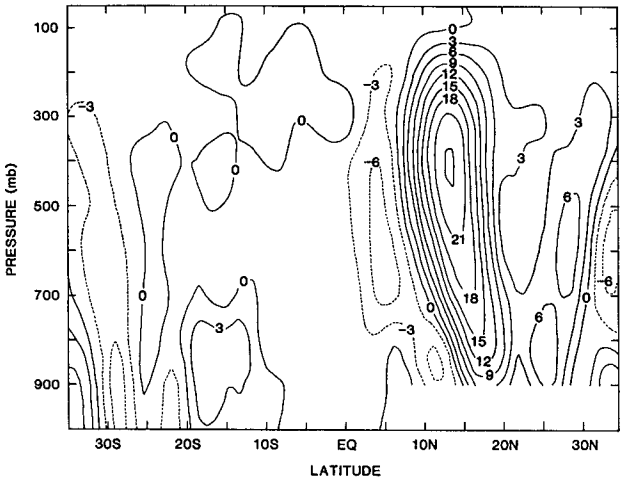

FIG. 12. The zonal average vertical wind (10^{-5} mb sec^{-1}) for experiments D minus C.

of the troposphere. Since the Africa easterly jet was stronger in experiment D, a linear instability consideration would have argued for stronger easterly wave disturbances. Apparently, the large-scale descent overwhelmed the linear instability giving rise to weaker waves. To the south of the test area there is an increase in the rising motion throughout the troposphere that is consistent with an increase in rainfall.

Figure 13a shows the wind vectors at 850 mb. It is seen that two contrasting flows exist over the sub-Sahara in the boreal summer in the lower troposphere: a warm moist flow that originates in the Southern Hemisphere, and a hot, dry flow that originates over the North Atlantic Ocean and the Mediterranean Sea. These two flows meet at the intertropical convergence zone (ITCZ). Over the African continent the ITCZ is to the north of the axis of maximum rainfall. The combined changes of zonal and meridional winds are shown in Fig. 13b, which is the vector wind difference between experiments D and C. It is clear that in the desertification case the moist airflow from the southern Atlantic Ocean became weaker and the hot dry flow from the northeast became stronger at the low level. The changes of the wind field and the reduced moisture field (not shown) affected the moisture convergence. The vertically integrated moisture flux convergence was reduced by about 1 mm day^{-1} in the test area (Fig. 14). The pattern in this figure is very similar to that in the rainfall difference (Fig. 4). The changes in moisture convergence and vertical motion above 800 mb (not shown) are consistent with changes in rainfall suggesting that the major cause of the rainfall deficiency was the change in the dynamical circulation.

c. *The impact of desertification on the surface energy balance and hydrology*

The changes in land surface characteristics altered the surface energy balance and hydrological cycle. The

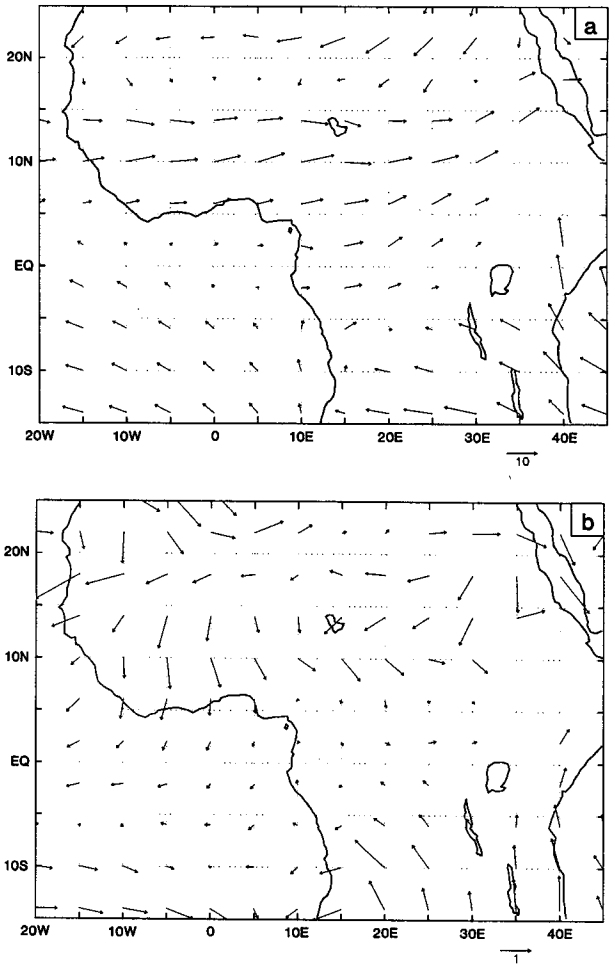

FIG. 13. Three-month mean wind vectors at 850 mb: (a) experiment C and (b) D minus C. Scale for speed (m s^{-1}) is shown at the bottom of each panel.

three-month means of various components of surface energy flux over the test area are listed in Table 3. The energy balance in these experiments is quite consistent with earlier experiments (Charney et al. 1977; Xue et al. 1990). In experiment D, the shortwave radiation

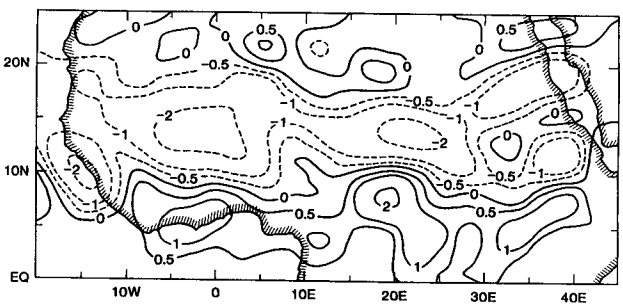

FIG. 14. Three-month mean moisture flux convergence (mm day^{-1}). Experiments D minus C.

TABLE 3. Energy balance at the surface for desertification (D), and control (C) experiments, and difference D–C.

	C	D	D–C
Surface albedo	0.21	0.3	0.09
Rainfall (mm day^{-1})	6.7	5.2	−1.5
Cloud cover	0.55	0.47	−0.08
Downward SWR at the surface (W m^{-2})	268	290	22
Absorbed SWR at the surface (W m^{-2})	211	203	−8
Downward LWR at the surface (W m^{-2})	396	389	−7
Upward LWR at the surface (W m^{-2})	464	468	4
Net (up) LWR at the surface (W m^{-2})	68	79	11
Surface temperature (K)	300.3	300.8	0.5
Sensible heat flux (W m^{-2})	68	68	0
Latent heat flux (W m^{-2})	82	63	−19
Interception loss (W m^{-2})	12	2	−10
Moisture flux convergence (mm day^{-1})	4.2	3.2	−1.0
Surface runoff (mm day^{-1})	0.4	1.0	0.6

reaching the surface was increased by 22 W m^{-2} due to a reduction in cloud cover (Fig. 15). The effects of a decrease in cloudiness and an increase in albedo compensated each other to give a small decrease (−8 W m^{-2}) in solar radiation absorbed at the surface (Fig. 16).

The downward longwave radiation was reduced due to lower cloud cover in D, and the net upward longwave radiation from the surface was increased by about 11 W m^{-2} (Fig. 17) because of a higher surface temperature. The anomaly patterns of longwave radiation loss at the surface and at the top of atmosphere over the test area in D were very similar.

The total radiation deficit of 19 W m^{-2} at the surface was balanced by a reduction in the latent heat flux. Figure 18 shows the difference in the latent heat flux due to desertification. The latent heat flux was reduced because of high albedo (less energy available to evaporate), lower surface roughness (less turbulent exchange), less soil moisture (reduced available water supply and increased soil surface resistance), and changes of other vegetation properties (such as vegetation cover). The reduction in evaporation (0.7 mm day^{-1}) was slightly less than half of the reduction in precipitation. Of this reduction in evaporation, 50%

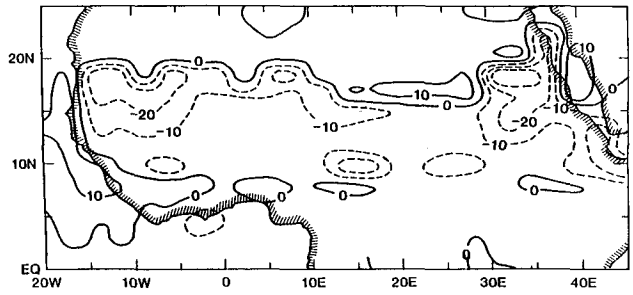

FIG. 16. Three-month mean for shortwave radiation absorbed at surface (W m^{-2}). Experiments D minus C.

was due to lower rainfall interception by the vegetation canopy, which in turn was due to less vegetation cover and less leaf area index in the desertification experiment. The reduction of rainfall and evaporation in the model simulations started at about the same time. There was negligible change in the sensible heat flux in D. Although we did not anticipate that there would be no change in the sensible heat flux, it is consistent with the fact that the surface temperature as well as the lower atmosphere temperature increased only slightly.

The surface temperature increased by about 0.5 K (Fig. 19). Only the area near 20°N and 30°E showed a large change in surface temperature because it was covered by tropical forest in the control case. In the test area, the atmospheric temperature increased below 700 mb and decreased between 700 mb and 300 mb (not shown). In most of the test area, the temperature at 850 mb increased by about 0.5 K with a maximum of 1 K. The reduction at upper levels was less than 0.5 K. Earlier studies have shown that the surface temperature increased in the Sahel during the dry years (Tanaka et al. 1975; Schupelius 1976; Kidson 1977). Tanaka et al. (1975) reported a surface air temperature increase of about 2 K, which was much larger than our model studies. The small increase of surface temperature in the desertification experiment is due to the compensating effects of increased albedo and reduced evaporation, which in turn is due to reduced vegetation, roughness length, and soil moisture.

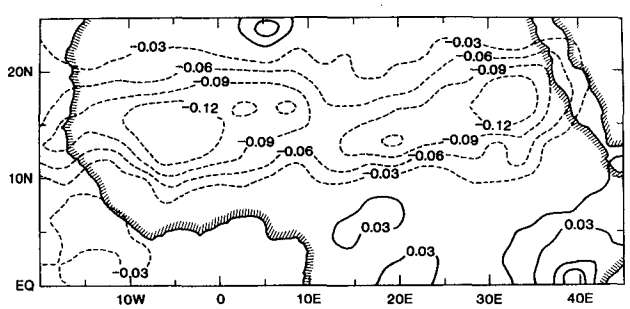

FIG. 15. Three-month mean for cloud cover. Experiments D minus C.

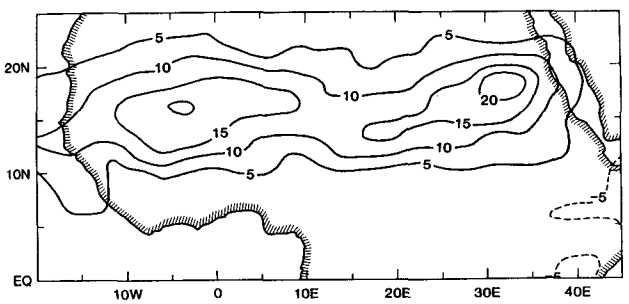

FIG. 17. Three-month mean for net longwave upward radiation at surface (W m^{-2}). Experiments D minus C.

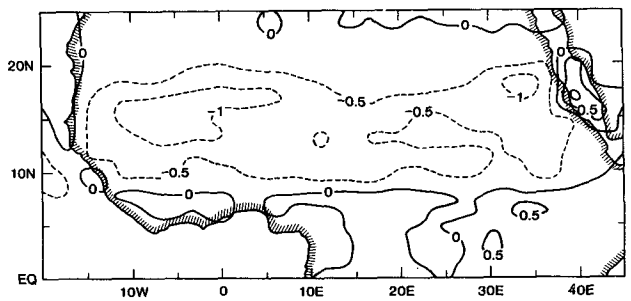

FIG. 18. Three-month mean for latent heat flux (W M^{-2}). Experiments D minus C.

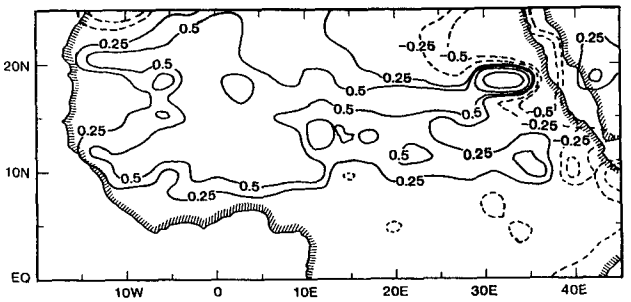

FIG. 19. Three-month mean for surface temperature (K). Experiments D minus C.

Table 3 shows that the reduction of rainfall (−1.5 mm day^{-1}) over the test area in D was less than the sum of decrease in moisture flux convergence (−1.0 mm day^{-1}) and evaporation (about −0.7 mm day^{-1}). In the desertification cases, the precipitable water in the atmosphere over the test area was reduced. Despite the reduced rainfall, the surface runoff increased by about 0.5 mm day^{-1}. This was because less rain was intercepted by the leaves, and the soil layer had less capacity to retain water. This result is consistent with observations in semiarid environments (Gornitz 1985). The soil moisture was also reduced in the desertification experiment. Figure 20 gives the difference of soil wetness in the surface layer. The soil wetness, which is the ratio of volumetric soil moisture in a soil layer to its value at saturation, was reduced in the entire test area.

5. Discussion and summary

This is a GCM sensitivity study to further explore the effects of desertification on the Sahel drought. A number of experiments have been carried out on this subject for more than a decade, which have shown a strong link between the land surface conditions and atmospheric circulation in this subtropical desert margin. In those studies only one or two parameters were arbitrarily changed. In this study, we have tried to more realistically prescribe the current Sahel desertification conditions. Since few measurements have been made of the changes of the physical surface characteristics (e.g., vegetation properties, albedo, surface moisture, surface roughness length) associated with land surface modifications, there is still not enough reliable data available to provide adequate information about the extent and degree of desertification in this region. We used vegetation type changes to represent desertification in our model simulations. The vegetation type replacement more or less reflects the "desert creep," a term used to describe the desertification in the sub-Sahara region (Dregne 1977). We changed the vegetation types in the region between about 10°N and 18°N. This change may exaggerate the actual situation in this region since desertification usually happens in patches. However, since we did not account for the desertification in the southern part of Ethiopia and near the Mediterranean coast, nor the deforestation near the Gulf of Guinea, the extent of our vegetation change region might be underestimated. Better assessments of the extent and magnitude of land surface changes would help to study more realistically the desertification effects on the Sahel climate.

The model used in this study gives a realistic simulation of the mean climate in general and the African rainfall pattern in particular. The results of this sensitivity study are in good agreement with previous similar studies providing further evidence for strong land surface influence on the regional climate. In order to reduce the sensitivity of results to the natural variability inherent in the GCM, five pairs of integrations were carried out, and the ensemble means of those cases were used to describe the final results. Since the most outstanding feature of the African climate anomaly is rainfall reduction, we have discussed in detail the impact of the desertification on rainfall in this paper. We found that the rainfall was reduced due to desertification and the rainy season was delayed by almost half a month. The axis of maximum rainfall shifted to the south. Thus, rainfall was increased to the south of the test area giving rise to a dipole rainfall anomaly pattern, which is in good agreement with the observations. The simulated seasonal mean rainfall anomalies caused by

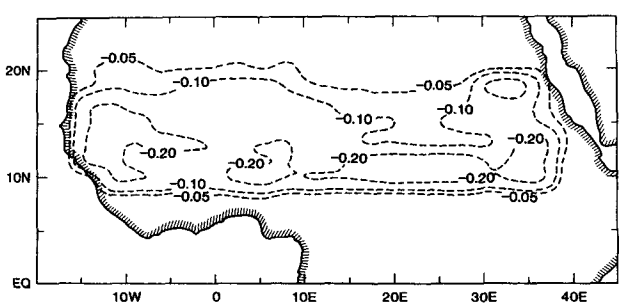

FIG. 20. Three-month mean for surface soil wetness. Experiments D minus C.

the land surface change were confined to the African continent only.

The African easterly jet (AEJ) and the monsoon from the Atlantic Ocean have significant influences on the Sahel summer rainfall, and both of them were sensitive to the land surface changes. The southwesterly moisture flow was weak in the desertification experiment. In agreement with Reed (1986), the westward disturbances had reduced intensity in desertification cases, but their number remained the same. Due to a warmer land surface in the desert region, a shallow rising area was simulated under the sinking air above.

The surface condition and atmospheric circulation changes led to the variation of the evaporation rate and the moisture flux convergence. In this study, the moisture flux convergence was reduced in the desertification cases. At least half of the reduction of the simulated evaporation was caused by the decrease of interception loss. The lack of vegetation preventing interception was earlier observed in the Amazonian rain forest (Shuttleworth et al. 1984). We have no observed data to quantitatively verify the interception loss in the Sahel region.

Finally, we would like to suggest that further numerical experiments with high-resolution models should be carried out to investigate the role of the land surface changes on the Sahel drought. Further experiments should include integrations for several annual cycles with observed sea surface temperature variations. Further experiments should also be carried out to investigate the sensitivity to changes in the size of the desertification area.

Acknowledgments. This research was supported by NASA Grants NAGW-1269, NAGW-557, and NSF ATM-9019296. We wish to thank Mike Fennessy for his assistance in numerical experiments, Drs. E. Rasmusson and P. Sellers for helpful discussions, and Dr. J. Kinter and Dr. A. J. Pitman for constructive suggestions to revise this manuscript. We are thankful to Dr. S. Nicholson for providing observed African rainfall data for four years, and Drs. D. Rowell, C. Folland, and T.-C. Yeh for their comments on an earlier manuscript. Special thanks go to M. Schlichtig for typing and T. Yeargin for editing this paper.

REFERENCES

Aubreville, A., 1949: Climates, forets, et desertification del'Afrique tropicale. Societe de editions geographiques. *Martime et coloniales.* 255 pp.

Burpee, R. W., 1975: Some features of synoptic-scale waves based on compositing analysis of GATE data. *Mon. Wea. Rev.*, **103,** 921–925.

Carlson, T. N., 1969: Some remarks on African disturbances and their progress over the tropical Atlantic. *Mon. Wea. Rev.*, **97,** 716–726.

Charney, J. G., 1975: Dynamics of deserts and drought in the Sahel. *Quart. J. Roy. Meteor. Soc.*, **101,** 193–202.

——, W. J. Quirk, S-H., Chow, and J. Kornfield, 1977: A comparative study of the effects of albedo change on drought in semi-arid region. *J. Atmos. Sci.*, **34,** 1336–1385.

Chervin, R. M., 1979: Response on the NCAR general circulation model to changed land surface albedo. Report of the JOC study Conf. on Climate Models, **Vol. 1,** GARP Pub., Ser. No. 22, WMO, 563–581.

Courel, M. F., R. S. Kandel, and S. I. Rasool, 1984: Surface albedo and the Sahel drought. *Nature,* **307,** 528–531.

Cunnington, W. M., and P. R. Rowntree, 1986: Simulations of the Saharan atmosphere-dependence on moisture and albedo. *Quart. J. Roy. Meteor. Soc.*, **112,** 971–999.

Davies, R., 1982: Documentation of the solar radiation parameterization in the GLAS Climate Model. NTIS No. N8230779, 57 pp.

Dennett, M. D., J. Elston, and J. A. Rodgers, 1985: A reappraisal of rainfall trends in the Sahel. *J. Climatol.*, **5,** 353–361.

Dregne, H. E., 1977: Desertification of arid lands. *Econ. Geogr.*, **53,** 322–331.

Dorman, J. L., and P. Sellers, 1989: A global climatology of albedo, roughness length, and stomatal resistance for atmospheric general circulation models as represented by the Simple Biosphere Model (SiB). *J. Appl. Meteor.*, **28,** 833–855.

Druyan, L. M., and R. D. Koster, 1989: Sources of Sahel precipitation for simulated drought and rainy seasons. *J. Climate,* **2,** 1438–1446.

Folland, C. K., T. N. Palmer, and D. E. Parker, 1986: Sahel rainfall and worldwide sea temperatures. *Nature,* **320,** 602–607.

——, J. Owen, M. N. Ward, and A. Colman, 1991: Prediction of seasonal rainfall in the Sahel region using empirical and dynamical methods. *J. Forecasting,* **1,** 21–56.

Gornitz, V., 1985: A survey of anthropogenic vegetation changes in west Africa during the last century—climate implication. *Clim. Change,* **7,** 285–235.

Harshvardhan, and T. G. Corsetti, 1984: Longwave radiation parameterization for the UCLA/GLAS GCM. NASA Tech. Memo. 86072, NTIS No. N8420971, 65 pp.

——, R. Davies, D. A. Randall, and T. G. Corsetti, 1987: A fast radiation parameterization for general circulation models. *J. Geophys. Res.*, **92,** 1009–1016.

Hou, Y.-T., 1990: Cloud-radiation-dynamics interaction. Ph.D. dissertation, University of Maryland, College Park, MD 20742. 209 pp.

Kidson, J., 1977: African rainfall and its relation to the upper air circulation. *Quart. J. Roy. Meteor. Soc.*, **103,** 441–456.

Kinter III, J. L., J. Shukla, L. Marx, and E. K. Schneider, 1988: A simulation of the winter and summer circulations with the NMC global spectral model. *J. Atmos. Sci.*, **45,** 2486–2522.

Kitoh, A., K. Yamazaki, and T. Tokioka, 1988: Influence of soil moisture and surface albedo changes over the African tropical rain forest on summer climate investigated with the MRI-GCM-I. *J. Meteor. Soc. Japan,* **66,** 65–85.

Kuo, H. L., 1965: On formation and intensification of tropical cyclones through latent heat release by cumulus convection. *J. Atmos. Sci.*, **22,** 40–63.

Lacis, A. A., and J. E. Hanson, 1974: A parameterization for the absorption of solar radiation in the earth's atmosphere. *J. Atmos. Sci.*, **32,** 118–133.

Lamb, P. J., 1978: Large-scale tropical Atlantic surface circulation patterns associated with sub-Saharan weather anomalies. *Tellus,* **30,** 240–251.

——, 1983: West African water vapor variations between recent contrasting Subsaharan rainy seasons. *Tellus,* **35,** 198–212.

——, and R. A. Peppler, 1991: West Africa. *Teleconnections Linking Worldwide Climate Anomalies,* M. Glantz, R. W. Katz and N. Nicholls, Eds., Cambridge University Press, 121–189.

Lanly, J. P., 1982: Tropical forest resources. *FAO Forestry Paper,* **30,** FAO, Rome, Italy, 106 pp.

Laval, K., and L. Picon, 1986: Effect of a change of the surface albedo of the Sahel on climate. *J. Atmos. Sci.*, **43,** 2418–2429.

Mellor, G. L., and T. Yamada, 1982: Development of a turbulence closure model for geophysical fluid problems. *Rev. Geophys. Space Phys.*, **20,** 851–875.

Newell, R. E., and J. W. Kidson, 1984: African mean wind changes between Sahalian wet and dry periods. *J. Climatol.*, **4,** 27–33.

Nicholson, S. E., 1979: Revised rainfall series for the west African subtropics. *Mon. Wea. Rev.*, **107,** 620–623.

——, 1981: Rainfall and atmospheric circulation during drought periods and wetter years in West Africa. *Mon. Wea. Rev.*, **109,** 2191–2208.

Norton, C. C., F. R. Mosher, and B. Hinton, 1979: An investigation of surface albedo variations during the recent Sahel drought. *J. Appl. Meteor.*, **18,** 1252–1262.

Philips, N., 1979: The nested grid model. NOAA Tech. Rep. NWS-22, NTIS No. PB299046, 79 pp.

Reed, R. J., 1986: On understanding the meteorological causes of Sahelian drought in persistent meteo-oceanographic anomalies and teleconnections, C. Chagas and G. Puppi, Eds., *Pontif. Acad. Sci.*, 179–213.

Rowell, D. P., and C. Blondin, 1990: The influence of soil wetness distribution on short-range rainfall forecasting in the west African Sahel. *Quart. J. Roy. Meteor. Soc.*, **116,** 1471–1485.

Sato, N., P. J. Sellers, D. A. Randall, E. K. Schneider, J. Shukla, J. L. Kinter, III, Y.-T. Hou, and E. Albertazzi, 1989: Effects of implementing the simple biosphere model in a general circulation model. *J. Atmos. Sci.*, **46,** 2757–2782.

Schupelius, G. D., 1976: Monsoon rains over West Africa. *Tellus,* **28,** 533–536.

Sela, J. G., 1980: Spectral modeling at the National Meteorological Center. *Mon. Wea. Rev.*, **108,** 1279–1292.

Sellers, P. J., Y. Mintz, Y. C. Sud, and A. Dalcher, 1986: A simple biosphere model (SIB) for use within general circulation models. *J. Atmos. Sci.*, **43,** 505–531.

Semazzi, F. H. M., V. Mehta, and Y. C. Sud, 1988: An investigation of the relationship between Sub-Sahara rainfall and global sea surface temperatures. *Atmos. Ocean,* **26,** 11 471–11 485.

Shukla, J., and Y. Mintz, 1982: Influence of land-surface evapotranspiration the earth's climate. *Science,* **215,** 1498–1501.

Shuttleworth, W. J., J. H. C. Gash, J. C. R. Lloyd, C. J. Moore, J. Roberts, Filho, A. de O. Marques, G. Fisch, V. de Paula Silva Filho, M. N. G. Ribeiro, L. C. B. Molion, L. D. de Abreu Sa, J. C. A. Nobre, O. M. R. Cabral, S. R. Patel, and J. C. de Moracs, 1984: Observation of radiation exchanges above and below Amazonia forest. *Quart. J. Roy. Meteor. Soc.*, **110,** 1163–1169.

Skoupy, J., 1987: Desertification in Africa. Agricultural and Meteorological Programs, *Proc. Regional Training Seminar on Drought and Desertification in Africa.* Addis Ababa, **33–45,** WMO.

Slingo, J. M., 1987: The development and verification of a cloud prediction scheme for the ECMWF model. *Quart. J. Roy. Meteor. Soc.*, **103,** 29–43.

Sud, Y. C., and M. Fennessy, 1982: A study of the influence of surface albedo on July circulation in semi-arid regions using the GLAS GCM. *J. Climate,* **2,** 105–125.

——, and ——, 1984: A numerical study of the influence of evaporation in semiarid regions on the July circulation. *J. Climatol.*, **4,** 383–398.

——, and A. Molod, 1988: A GCM simulation study of the influence of Saharan evapotranspiration and surface-albedo anomalies on July circulation and rainfall. *Mon. Wea. Rev.*, **116,** 2388–2400.

Tanaka, M., B. C. Weare, A. R. Navato, and R. E. Newell, 1975: Recent African rainfall patterns. *Nature,* **255,** 201–203.

Verstraete, M. M., 1986: Defining desertification: A review. *Clim. Change,* **9,** 5–18.

Walker, J., and P. R. Rowntree, 1977: The effect of soil moisture on circulation and rainfall in a tropical model. *Quart. J. Roy. Meteor. Soc.*, **103,** 29–46.

Xue, Y., 1991: A two-dimensional coupled biosphere-atmosphere model and its application. *Adv. in Atmos. Sci.*, **8,** 447–458.

——, K. N. Liou, and A. Kasahara, 1990: Investigation of the biogeophysical feedback on the African climate using a two-dimensional model. *J. Climate,* **3,** 337–352.

——, P. J. Sellers, J. L. Kinter III, and J. Shukla, 1991: A simplified biosphere model for global climate studies. *J. Climate,* **4,** 345–364.

Yeh, T.-C., R. T. Wetherald, and S. Manabe, 1984: The effect of soil moisture on the short-term climate and hydrology change—a numerical experiment. *Mon. Wea. Rev.*, **112,** 474–490.